Modeling of Non-Newtonian Polymer Flooding with Adsorption and Retention Using Parametrization Approach

Lyu, X.; Voskov, D.V.; Mao, J.

DOI
10.3997/2214-4609.202244013

Publication date
2022

Document Version
Final published version

Published in
European Conference on the Mathematics of Geological Reservoirs 2022

ECMOR 2022
European Conference on the Mathematics of Geological Reservoirs

EAGE

Modeling of Non-Newtonian Polymer Flooding with Adsorption and Retention Using Parametrization Approach

X. Lyu[1], D. Voskov[2,3], J. Mao[2]

[1] China University of Petroleum-Beijing; [2] Delft University of Technology; [3] Stanford University

Summary

Polymer flooding is one efficient EOR technology by overcoming non-uniform and unstable displacement caused by water injection. Polymer flooding in reservoirs is a complicated process that involves strongly nonlinear physics, e.g., non-Newtonian rheology in porous media with retention and adsorption. In the presence of multi-scale heterogeneity, high-fidelity simulations are usually required to capture such nonlinear behavior, which is a time-consuming process for conventional reservoir modelling.

In this study, we extend an advanced linearization strategy, called the Operator-Based Linearization (OBL) approach, to simulate non-Newtonian polymer flooding with retention and adsorption mechanisms using the fully implicit method. A velocity-dependent viscosity multiplier compliments the operator form of governing equations to represent the non-Newtonian rheology of the high-molecular-compound polymer. The retention of polymer, reducing the porosity, is represented by a Langmuir-type adsorption model. Several simplified models have been used for validation of the developed numerical framework. The numerical results show good agreement with both the analytical solutions and the coreflood experimental data though some negligible discrepancies can be observed in simulation results.

A highly resolved near-well model is used to test the performance of polymer flooding in realistic reservoir conditions. Both shear-thinning and thickening regimes, depending on the injection velocity and polymer concentration, are recognized in the near-wellbore zone. The injected polymer concentration and brine salinity significantly affect the shear viscosity, and consequently, polymer injectivity. Polymer retention and adsorption have a substantial effect on the rate of polymer propagation through porous media. Overall, polymer flooding shows its advantages to mitigate water fingering in field-scale operations and improves the ultimate sweep of the reservoir. However, optimal injectivity is one essential factor that affects the performance of polymer flooding. The computational superiority of the proposed model allows us to optimize the parameters of polymer flooding in realistic reservoirs and operational settings.

Introduction

Polymer flooding, one of the most widely used chemical enhanced oil recovery (CEOR) techniques, has attracted great interest due to its unique advantages compared to other EOR methods (Needham and Doe, 1987; Kamal et al., 2015). Applying polymer flooding enables the scope of economically accessible prospects to expand: high-viscosity polymers overcome non-uniform and invalid displacement caused by water fingering, which extends polymer flooding to high-permeability and heavy-oil reservoirs (Firozjaii and Saghafi, 2020). In addition, polymers prepared from formation water with low mineralization and low hardness exhibit excellent thermal stability, which extends polymer flooding to high-temperature and high-mineralized reservoirs (Vermolen et al., 2011). The current polymer flooding screening standards state that polymer flooding is applicable in crude oil production with low viscosity, moderate temperature, and in formations with extremely severe horizontal and vertical heterogeneity (Saleh et al., 2014).

Nowadays, the focus of research is on the development of polymers with good water solubility, strong thickening ability, salt tolerance, thermal and shear resistance, stability to biological and chemical factors, low retention, wide availability, and low cost (Sheng et al., 2015). For example, hydrophobically associating water-soluble polymer (HAWP) with a small number of hydrophobic groups promoting intermolecular association resists viscosity loss in saline reservoirs(Hill et al., 1993); cross-linked polymer made of HPAM coupled with aluminium citrate can selectively seal near-well and internal formations by switching between the bulk gel and linked polymer solution (LPS) under different polymer concentration (Shiran and Skauge, 2014).

Numerical simulation is an important tool that predicts the polymer dynamic characteristics in porous media (Yuan et al., 1995). Based on a reasonable description of displacing mechanism as well as physical and chemical phenomena, accurate simulation and prediction of the polymer flooding process can be accomplished. This, in turn, can minimize the investment risks while maximizing the economic benefits. Some researchers have conducted laboratory experiments or field pilots to understand the complicated polymer rheology and the mechanics of polymer EOR in porous media. However, numerical simulations including polymer rheology and flow are relatively rare due to the high complexity of physical phenomena and their implementation in a simulation framework.

Currently, the representative polymer flooding numerical simulators include VIP- POLYMER (Landmark), ECLIPSE100 (Schlumberger), STAR (CMG), ASP (RIPED), UTCHEM (UTA). The following characteristics are drawn from the simulators stated above Liu et al. (2012):

- The number of involved components increases in the polymer flooding which brings the need for the higher-order discretization and solution of more complex nonlinear equations. At present, all the numerical simulators for polymer flooding are much slower in comparison to water flooding simulators. As a result, the scale of polymer flooding simulation is greatly restricted.
- When the number of added components in the polymer flooding is small, the fully-implicit method is preferred which can effectively guarantee the stability of the simulation. However, certain physical and chemical parameters require a large number of components to represent the results of laboratory study. Therefore, trade-offs between stability and rationality of the physical representation have to be faced.
- The theory of viscoelasticity reducing the remaining oil was proposed, but it has not been taken into account by mainstream simulation software. The main difficulty lies in how to incorporate the microscopic viscoelastic theory into the macroscopic grid concept.
- The commonly used numerical models do not consider the issue of non-isothermal polymer degradation. The obstacle is present in how to access the value of polymer degradation and the development of an efficient non-isothermal waterflooding model.
- The improved black oil model is still the leading choice for polymer flooding today. The advantages are simplicity and ease of use, relatively small computational time and less storage space

required; the disadvantage is that it cannot express the multi-component mass changes completely caused by interphase exchange and the resulting changes in fluid properties and flowing states.

- The compositional model allows a more accurate description of various physical phenomena and chemical reactions to be reflected in the change of composition. However, the computational overhead is often very large, which limits the implementation.

The research objective of this study is to construct an efficient model for polymer flooding, which requires a realistic reflection of the complicated physical behaviour of polymer in porous media, including the rheology and retention phenomenon exclusive to high-molecular compounds. First, the modelling details are described, including the system of conservation equations, polymer rheology and retention models. The numerical framework is briefly introduced next. Then the numerical simulations are carried out to investigate the complicated flow behavior of polymer in porous media. Finally, based on computed tomography (CT) images, we construct a more-accurate 3D heterogeneous model to represent the core utilized in the experiment. This high-fidelity 3D model is used to reproduce the displacement experiments. The developed simulator shows good performance with improved accuracy and flexibility.

Mathematical model

Basic Conservation Equations and Operator Based Linerization Framework

The general mass balance equations, which are used to describe multi-phase multi-component flow in porous media, can be rewritten in Eq. 1

$$\frac{\partial}{\partial t}\left(\phi\sum_j x_{cj}\rho_j s_j\right)+\nabla\sum_j(x_{cj}\rho_j\overrightarrow{u_j})+\sum_j x_{cj}\rho_j\widetilde{q}_j=0, \tag{1}$$

where the subscript j and c refers to the phases and components respectively, x_{cj} is the mole fraction of component c in phase j. The phase velocity, $\overrightarrow{u_j}$, is described by Darcy's law (Eq. 2)

$$\overrightarrow{u_j}=-K_{abs}\frac{k_{rj}}{\mu_j}(\nabla p_j-\rho_j g\nabla D), \tag{2}$$

where K_{abs} is the absolute permeability within the porous media, k_{rj} is the relative permeability of phase j which correlates with saturation, and D is the reservoir depth.

The expressions of all variables can be regrouped into the product of state-dependent (ω) operators, keeping in line with the OBL approach (Voskov, 2017; Lyu et al., 2021)

$$R_i(\omega)=V\phi_0(\alpha_c(\omega)-\alpha_c(\omega_n))-\Delta t\sum_{l\in L}T^l\beta^l_{cj}(\omega)\Delta\Phi^l. \tag{3}$$

Hereby ω and ω_n are physical states (p and z_c) for current and previous timesteps, respectively; l is one of the interfaces in a control volume with L interfaces, and $\Delta\Phi$ is the pressure difference of interface l. V is the control volume, T^l is the transmissibility between neighbouring grid-blocks. To tackle the given governing equation (Eq. 3), the fully-implicit method (FIM) is put into operation. To arrange the terms in residual form, the mass-conservation equation is discretized by backward Euler.

Considering the possibility of miscible flooding, summation of each phase should be created in a loop with all the phases j present. The operators that break up the cumbersome nonlinear functions are defined as the following set of relations (from Eq. 4 to Eq. 5)

$$\alpha_c(\omega)=(1+c_r(p-p_{ref}))z_c\rho_T, \tag{4}$$

$$\beta^l_{cj}(\omega)=\sum_{j=1}^{2}x_{cj}\rho_j\frac{k_{r,j}}{\mu_j}, \tag{5}$$

Here c_r is rock compressibility, ω is the bundle of state-related unknowns variables.

Polymer Rheology

The viscosity of the flowing polymer solution is the direct target of shear rate and shear stress, two principle parameters that typify the rheological features of the system. At a certain temperature (such as reservoir temperature), the viscosity of polymer solution (μ_{aq}) mainly varies with polymer concentration (C_p [ppm]), and shear rate ($\dot{\gamma}$ [s^{-1}]) as Eq. 6

$$\mu_{aq} = \mu_{aq}(\mu^0_{aq}, \dot{\gamma}), \tag{6}$$

where $\mu^0_{aq}$is viscosity of polymer solution at zero shear rate ($\mu^0_{aq} = \mu_{aq}|_{(\dot{\gamma}\to 0)}$) that depends on C_p.

An explicit discretization method is adopted for addressing the viscosity in polymer flooding, in which the sequential simulation of subproblems is placed outside the entire Newton scheme while wrapped in the full-time loop as shown in Fig. 1. This scheme can be described in the following steps:

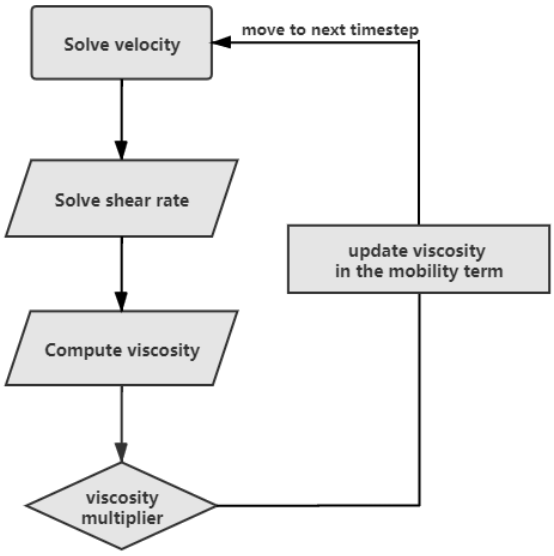

Figure 1 *Flow chart of viscosity calculation.*

1. Compute u_{aq} at timestep v in Eq.7

$$u^v_{aq} = -\frac{k_{abs}k^v_{r,aq}}{{\mu^0_{aq}}^v M^v}\nabla p^v. \tag{7}$$

   Here the state-dependent properties $k^v_{r,aq}$, μ^0_{aq}, M^v and spatial variable (∇p) are all calculated in v_{th} timestep, M is a array of viscosity multiplier, defined in Eq. 11.

2. Compute $\dot{\gamma}$ and ${\mu^0_{aq}}^v$ in Eq. 8,

$$\dot{\gamma}^v = C(\frac{3n+1}{4n})^{\frac{n}{n-1}}\frac{{u_{aq}}^v}{\sqrt{K{k_{r,aq}}^v{S_{aq}}^v\phi}}. \tag{8}$$

   Here ${u_{aq}}^v$ and ${k_{r,aq}}^v$ are the Darcy velocity and relative permeability of aqueous phase respectively, ${S_{aq}}^v$ is the aqueous saturation, and C is the shear correction factor. When C is equal to 6, it is claimed that the Eq. 8 matches a wide variety of core flood data. The zero-shear viscosity can be expressed in Eq.9

$${\mu^0_{aq}}^v = \mu_w(1+(a_1C^v_p + a_2C^{v2}_p + a_3C^{v3}_p)C^{SP}_{SEP}), \tag{9}$$

   where μ_w is the water viscosity and a_1, a_2, a_3 and S_p are coefficients obtained from experiments.

3. Compute μ_{aq}^{v} at timestep v based on Eq. 10

$$\mu_{aq}^{v} = \mu_w + (\mu_{aq}^{0\ v} - \mu_w)[1 + (\lambda\dot{\gamma}^{v})^2]^{\frac{n-1}{2}} + \mu_{max}[1 - exp(-\lambda_2\tau_r\dot{\gamma}^{v})^{n_2-1}]. \tag{10}$$

where the 8-parameter Delshad's model (Delshad et al., 2008), captures the Newtonian plateaus at low, shear-thinning behaviour at intermediate shear rates, and shear-thickening uplift at high shear rate. The other elements are all constant parameters exclusive of the only variable $\dot{\gamma}$. Here $\mu_{aq}^{0\ v+1}$ and $\mu_{aq}^{0\ v}$ are the polymer viscosity under apparent and zero shear rate, respectively, μ_w is viscosity of water, and λ, n, n_2, λ_2, μ_{max} and τ_r are experiment fitted constants from laboratory.

4. Compute M at timestep v (Eq. 11). Viscosity multiplier is defined as a ratio of apparent viscosity at timestep $(v+1)$ to the zero shear-rate viscosity at timestep v as Eq. 11. The M is set to be 1 as the original state, namely 0 timestep

$$M^{v} = \frac{\mu_{aq}^{v}}{\mu_{aq}^{0\ v}}. \tag{11}$$

5. Update the u_{aq} at timestep $v+1$ employing Eq. 12

$$u_{aq}^{v+1} = -\frac{k_{abs}k_{r,aq}^{v+1}}{\mu_{aq}^{0\ v+1}M^{v}}\nabla p^{v+1}. \tag{12}$$

As the simulation keeps iterating, the zero-shear viscosity at the current step is updated by multiplying with the viscosity multiplier from previous timestep. This scheme can also be complemented by an implicit treatment of velocity.

Polymer Retention Model

A Langmuir isotherm is the most common approach to model adsorption in the polymer flooding (Hirasaki and Pope, 1974). Langmuir makes the assumption of a uniform surface of the adsorbent and equlibrium treatment for the energy of adsorption. Monolayer adsorption treatment yield the maximum adsorption capacity as soon as the adsorbent surface is saturated with adsorbates,. Whereby, the adsorbed concentration of polymer is given by a function of polymer concentration as Eq. 13,

$$C_a = min(C_p, \frac{aC_p}{1+bC_p}), \tag{13}$$

where C_p and C_a [wt%] are the polymer concentrations flowing at the pores and trapped on the stationary phases. The placement of minimum in Eq. 13 is taken to guarantee the mass balance in case the adsorption amount (second term) surpasses the injected polymer amount (first term) after 100% saturation. The Langmuir's coefficient a and b are input coefficients fitted from the experiments, which can vary due to the salinity and permeability changes. However the effect of ions and permeability is not going to be discussed in this study.

Using the density of the polymer as a bridge, the adsorption concentration can be converted to volume of the adsorbed polymer and update the porosity as following Eq. 14

$$\phi_{new} = \phi_{ini} - \frac{aC_p(1-\phi_{ini})}{(1+bC_p)\rho_p}, \tag{14}$$

where ϕ_{ini} is the post-compressed porosity at subsurface pressure, C_p is the flowing polymer concentration, ρ_p is the polymer density.

Due to the shrinking of the effective size of the pores caused by adsorption and retention of the polymer molecular coils, the formation permeability decreases. Two dimensionless quantities, the permeability reduction factor (R_k) and the residual resistance factor (R_{rf}) are formulated for the aqueous phase to

describe the permeability reduction quantitatively. R_k is the ratio of effective permeability of aqueous phase before and after polymer injection. R_{rf} stands for the ratio of the size of the polymer molecular coil to the effective pore diameter of the porous medium, which is formulated to correlate the reduction of permeability with rock properties (Choi et al., 2015).

The permeability reduction factor is linearly proportional to the degree of polymer adsorption, and both of the two climb to a max amount as described in Eq. 15

$$R_k = 1 + (R_{k,max} - 1)\frac{\hat{C}_p}{C_{p,max}}, \tag{15}$$

where $R_{k,max}$ is the maximum permeability reduction factor, $\hat{C}_p$ is the adsorbed level of polymer ($gmole/m^3$) and $C_{p,max}$ is the maximum adsorption capacity ($gmole/m^3$).

For a homogeneous capillary-tube model (regardless of the anisotropy of permeability), the permeability change is analogous to the reduction of the capillary radius on the basis of the Hagen-Poiseuille law (Kang et al., 2018), which is derived as Eq. 16

$$R_{k,max} = min\left(\left[1 - \frac{c_{rk}[\mu_p]^{\frac{1}{3}}}{\frac{k}{\phi}^{\frac{1}{2}}}\right]^{-4}, rkcut\right), \tag{16}$$

where c_{rk} is the input parameter obtained from laboratory, μ_p is the intrinsic polymer viscosity and *rkcut* acts as the upper bound of permeability reduction. As an additional parameter to lower mobility besides viscosity increase, the viscosity of aqueous phase is multiplied by R_k to involve the effect of channel blocking during the simulation.

Results and Discussions

A near-well model is built to test the performance of polymer rheology. Both shear-thinning and thickening regimes, depending on the injection velocity, polymer concentration and the brine salinity are recognized in the near-wellbore zone. The parameters are listed in Table. 1.

Table 1 *Simulation settings for HPAM rheology validation.*

Parameter	Values
Injected polymer concentration	(3330 ppm,1667 ppm,167 ppm)
Bottomhole Pressure at injection well	(500, 300, 230) bars
Zero-shear viscosity parameters Ap_1, Ap_2, Ap_3	40, 0, 0
The parameters considering the effect of salinity C_{SEP}, S_p	1, 0
Shear thinning model parameters β_1, β_2, n_1	0.25, 0.5, 0.9
Shear thickening model parameters AP_{11}, AP_{22}, τ_0, τ_1, n_2, and λ_2	0.1, 0.01, 3000, 1500, 2, 1×10^{-7}

Effect of Injected Polymer Concentration

As shown in Fig.2, the viscosity is found to decrease at a lower shear rate, while starts to increase with a greater shear rate, which is corresponding to the shear-thinning and shear-thickening regimes, respectively, dominated by the injection velocity. With a lower concentration, the viscosity of polymer nearly shows a constant value. The lower the mass concentration of polymer molecules, the fewer molecules in the aqueous solution, leading to a lower likelihood of molecular chains or coils intertwining and permeating each other. Consequently, there is no perceived increase in the viscosity of the polymer at a lower injection concentration. In addition, the pseudo-plasticity of the polymer (the lowering viscosity decreases as the shear rate is small) and the viscoelasticity (the rebounding viscosity as the shear rate increases within the relaxation time) are both captured. It indicates that an approximate polymer concentration should be contrived to achieve a better performance.

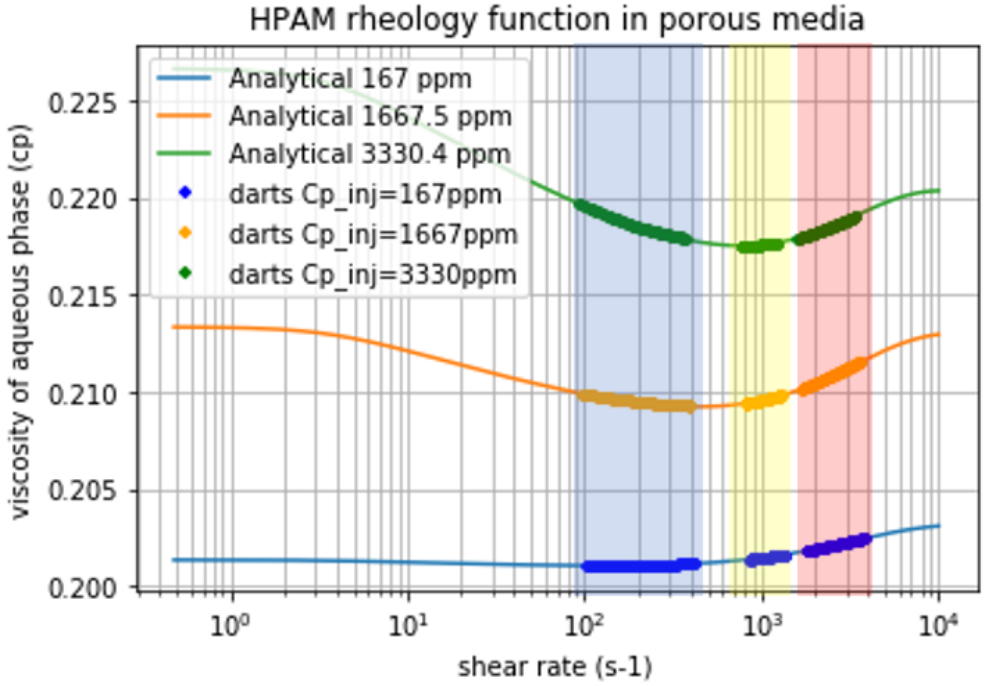

Figure 2 *Analytical and numerical solutions of polymer rheology in porous media at different concentrations. The solid curves present the unified analytical model while the discretized points present the numerical results. The three blocks in light blue, yellow and pink mark the three intervals of shear rates when the pressure at injection well is 230bar, 300bar and 500bar respectively.*

Effect of Brine Salinity

When the salinity degree is rising, the intramolecular and intermolecular hydrogen bonds are forming between positive and negative ion groups, resulting in the decrease of the solubility of the polymer in water. At the same time, the additional ions from salt shield the positive and negative charges, allowing them to scatter. The formation of salt bonds is destroyed when negative ions come together, leading to an increase in the solubility of the polymer in water. These two actions cancel each other out, hence the polymer's viscosity-increasing impact at higher salt concentrations is zero as observed in Fig. 3. That is, the apparent viscosity of the polymer solution flattens out and is infinitely close to the solvent viscosity.

Simulation of Core Experiments

A 3D heterogeneous simulation grid is established based on the CT images, as is presented in Fig. 4(b). The porosity of each pixel and each CT slice has been corrected by use of the following formula (Sharma et al., 1997).

$$\phi = \frac{CT_{water} - CT_{air}}{CT_w - CT_a} \tag{17}$$

where CT_{water} and CT_{air} are the CT values of a core completely soaked with water and a unsaturated core filled with air respectively; CT_w and CT_a are CT values of water and air, respectively.

Following these relations, porosity of each triangular grid block can be obtained. As the slice shown in Fig. 4 (a), the porosity is distributed in an unstructured network composed of 1,080 grids with an average area of 1.16 mm^2. Correspondingly, the permeability can be computed using the Kozeny-Carman equation (Eq. 18)

$$k = \alpha \frac{\phi^3 D_p^2}{(1-\phi)^2}, \tag{18}$$

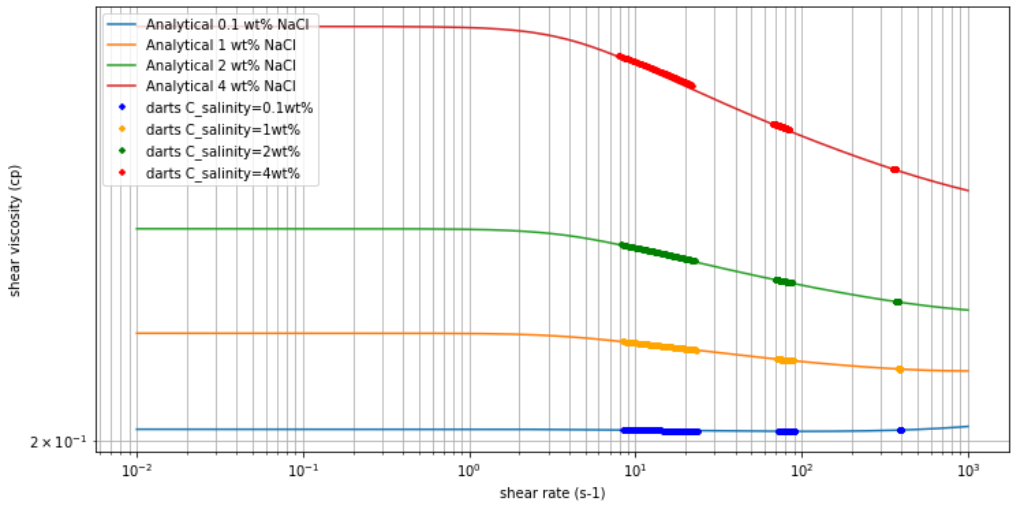

Figure 3 *Analytical solution and numerical solution of HPAM rheology in porous media affected by different salinity of 0.1wt%, 1wt%, 2wt% and 4wt%. The continuous curves present the unified analytical model while the discretized points present the numerical results implemented by DARTS. The three intervals of shear rates when the pressure at injection well is 215bar, 230bar and 300bar respectively.*

where k refers to the absolute permeability in md; D_p denotes the average diameter of sand grains in mm; ϕ symbolizes the porosity of the core, with the unit in fraction and α stands for the combined proportionality and unity factor in unit of md/mm^2.

The permeability is assumed to share the same distribution pattern and frequency with the porosity. This assumption allows the overall permeability and porosity distribution to be solved applying the group of α and D_p^2 extracted from the relationship between the known average porosity and average permeability.

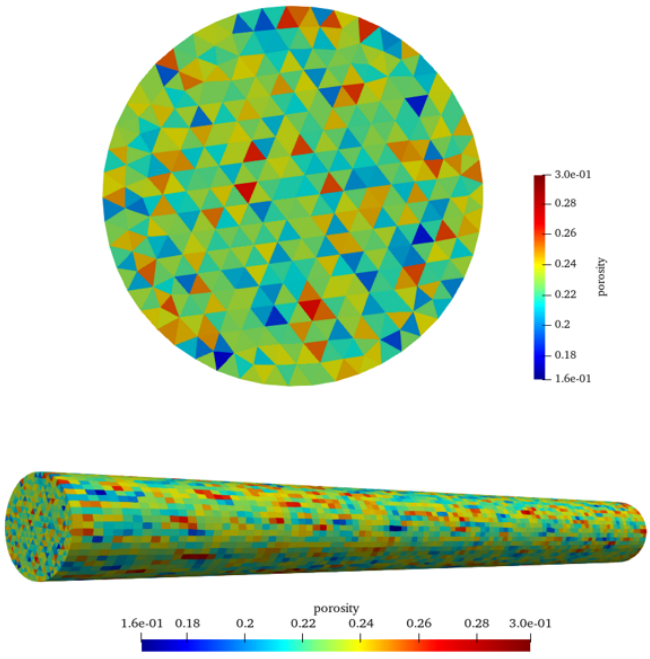

Figure 4 *Porosity profile of Bentheimer sandstone at a slice and along the core.*

The injection inlet and the production outlet locate at the far left and right ends respectively of the core and all unstructured grids at the two ends of the slice are connected with them. After 0.82 PV injection, the water molar fraction is far smaller if polymer is present because the polymer flood slows down the propagation of the water in the core due to the increased water viscosity. Consequently, the oil molar fraction at the production well with polymer is higher than the oil molar fraction of the case without injection of polymer, confirming that the physical properties of polymer injections which aims to increase swept surfaces and reduce the displacement rate.

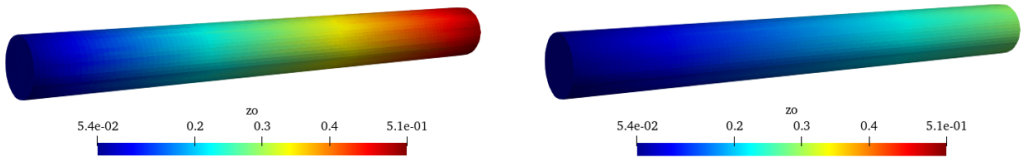

Figure 5 *The molar fraction of oil when injecting a) 1×10^{-8} mol/mol (1667ppm) and b) no polymer at 3×10^{-5} days.*

Except for the obvious effect of the concentration of injected polymer as the flowing retardation of water, the injected polymer concentration also exerts an important effect on polymer adsorption and porosity reduction. As shown in Fig. 6(a) to 6(c), it can be seen that as the injected polymer concentration decreases, the constant part with larger porosity, where polymer solution sweeps (i.e., inlet side), gradually becomes shorter, while the transition zone and the another constant part with relatively smaller porosity become longer. It can be regarded as three stages: the first stage occurs when the polymer concentration is injected at its maximum, resulting in over-saturated state and a maximum porosity reduction factor. The second stage occurs when the polymer shock appears, causing the increasing percentage of retained polymer to all of the injected polymer which lasts until the third stage occurs where polymer becomes undersaturated.

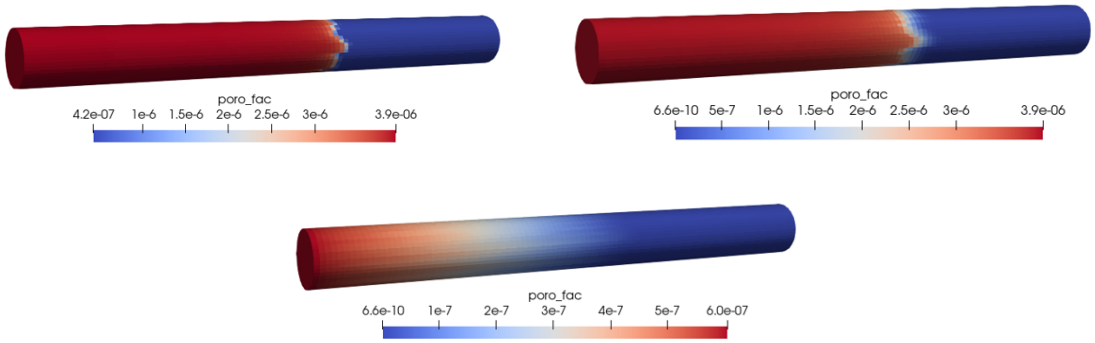

Figure 6 *The porosity reduction factor distribution at injected polymer concentration of 1664 ppm (1×10^{-8}mol/mol), 16.6 ppm (1×10^{-10}mol/mol), and 1.66 ppm (1×10^{-12}mol/mol) serves as the only variable. Hereby the upper bound of polymer retention is set to be 1, with a and b both set to be 5.*

As the polymer concentration drops, it is no longer possible for the polymer to maintain the upper bound of adsorption, resulting in a gradual increase in the transition period between oversaturation (first stage) and undersaturation (third stage). Simultaneously, the critical point (between the second and the third stage) is achieved earlier, leading to a longer third stage of undersaturation.

Conclusions

In this work, the conservation equation is solved by Fully Implicit Method using the Operator-Based Linearization framework, a more stable and less costly approach to deal with the associated physics of polymer.

The obtained model achieves to present the phenomenon of rheological behaviour and retention of polymer. To better present the nature of shear-viscosity and elongational viscosity, a unified viscosity model for polymer flooding involving a full spectrum of Newtonian, shear-thinning, and shear-thickening flowing behaviour of polymer solutions is successfully implemented in the Delft Advanced REserach Terra Simulator (DARTS). For polymer retention, the influence of retained polymer macromolecules on porosity reduction (besides permeability reduction) is investigated and has a perfect response with the principle of Langmuir isotherm adsorption.

The polymer flooding simulation of core lab experiments is put into practice using a heterogeneous core structure reconstructed from CT imaging. In this way, a more close-to-reality behavior usually observed in lab experiments is reproduced by the model. This simulation can serve as a source for an accurate upscaling of core flooding results to reservoir scale.

Acknowledgments

We acknowledge the financial support of Science Foundation of China University of Petroleum, Beijing (No.2462022BJRC003) and National Natural Science Foundation of China Joint Fund Project (No.U20B6003).

References

Choi, B., Choi, J. and Lee, K.S. [2015] Integrated analysis of permeability reduction caused by polymer retention for better understanding polymer transport. *Journal of Chemistry*, **2015**.

Delshad, M., Kim, D.H., Magbagbeola, O.A., Huh, C., Pope, G.A., Tarahhom, F. et al. [2008] Mechanistic interpretation and utilization of viscoelastic behavior of polymer solutions for improved polymerflood efficiency. In: *SPE Symposium on Improved Oil Recovery*. Society of Petroleum Engineers.

Ding, L., Wu, Q., Zhang, L. and Guérillot, D. [2020] Application of fractional flow theory for analytical modeling of surfactant flooding, polymer flooding, and surfactant/polymer flooding for chemical enhanced oil recovery. *Water*, **12**(8), 2195.

Firozjaii, A.M. and Saghafi, H.R. [2020] Review on chemical enhanced oil recovery using polymer flooding: Fundamentals, experimental and numerical simulation. *Petroleum*, **6**(2), 115–122.

Hill, A., Candau, F. and Selb, J. [1993] Properties of hydrophobically associating polyacrylamides: influence of the method of synthesis. *Macromolecules*, **26**(17), 4521–4532.

Hirasaki, G. and Pope, G. [1974] Analysis of factors influencing mobility and adsorption in the flow of polymer solution through porous media. *Society of Petroleum Engineers Journal*, **14**(04), 337–346.

Kamal, M.S., Sultan, A.S., Al-Mubaiyedh, U.A. and Hussein, I.A. [2015] Review on polymer flooding: rheology, adsorption, stability, and field applications of various polymer systems. *Polymer Reviews*, **55**(3), 491–530.

Kang, C., Jung, K., Lee, M. and Jang, G. [2018] Finite-element coupled analyses of the Reynolds and Hagen–Poiseuille equations to calculate pressure and flow of fluid dynamic bearings with a recirculation channel. *Tribology International*, **128**.

Liu, W.l., MA, D.s., WANG, Q. and Liu, Z.x. [2012] Numerical simulation for chemical flooding [J]. *Journal of Daqing Petroleum Institute*, **3**.

Lyu, X., Khait, M. and Voskov, D. [2021] Operator-Based Linearization Approach for Modeling of Multiphase Flow with Buoyancy and Capillarity. *SPE Journal*.

Needham, R.B. and Doe, P.H. [1987] Polymer flooding review. *Journal of petroleum technology*, **39**(12), 1503–1507.

Saleh, L.D., Wei, M. and Bai, B. [2014] Data analysis and updated screening criteria for polymer flooding based on oilfield data. *SPE Reservoir Evaluation & Engineering*, **17**(01), 15–25.

Sharma, B.C., Brigham, W.E. and Castanier, L.M. [1997] CT imaging techniques for two-phase and three-phase in-situ saturation measurements. Tech. rep., Stanford Univ., CA (United States).

Sheng, J.J., Leonhardt, B. and Azri, N. [2015] Status of polymer-flooding technology. *Journal of Canadian petroleum technology*, **54**(02), 116–126.

Shiran, B.S. and Skauge, A. [2014] Similarities and differences of low salinity polymer and low salinity LPS (linked polymer solutions) for enhanced oil recovery. *Journal of dispersion science and technol-*

ogy, **35**(12), 1656–1664.
Vermolen, E., Van Haasterecht, M., Masalmeh, S.K., Faber, M.J., Boersma, D.M. and Gruenenfelder, M. [2011] Pushing the envelope for polymer flooding towards high-temperature and high-salinity reservoirs with polyacrylamide based ter-polymers. In: *SPE middle east oil and gas show and conference*. OnePetro.
Voskov, D. [2017] Operator-based linearization approach for modeling of multiphase multi-component flow in porous media. *Journal of Computational Physics*, **337**, 275–288.
Yuan, S., Yang, P., Dai, Z., Shen, K. et al. [1995] Numerical simulation of alkali/surfactant/polymer flooding. In: *International Meeting on Petroleum Engineering*. Society of Petroleum Engineers.

Appendix

We use the Corey relative-permeability model in this study. The relative-permeability data of Ding et al. (2020) is used for validating our simulator and investigate the effect of different parameters on polymer rheology:

$$k_{ro} = 0.40\left(\frac{1 - S_w - S_{or}}{1 - S_{wc} - S_{gr}}\right)^2, \tag{19}$$

$$k_{rw} = 0.14\left(\frac{S_w - S_{wc}}{1 - S_{wc} - S_{gr}}\right)^4, \tag{20}$$

$$f_w = \frac{1}{1 + \frac{k_{rg}(S_w)}{\mu_g}\frac{\mu_w}{k_{rw}(S_w)}}. \tag{21}$$

In this model, S_{wc}=0.15, and S_{gr}=0.24. The following values are assumed for physical properties in Eq. 21: μ_w = 0.5 cp, μ_p = 30 cp and μ_o = 72 cp.

As shown in Fig. 7, there are two shocks present: the oil bank front, behind which the initial water in the system displaces oil and the chemical front behind which the injected chemical pushes the oil toward the outlet. Behind the polymer shock, it is a region of spreading waves with constant polymer concentration. Before water breakthrough, pure oil is produced and the initial oil saturation does not influence the polymer front. From this comparison, we validate our simulator against the analytical solution obtained from the fractional-flow theory.

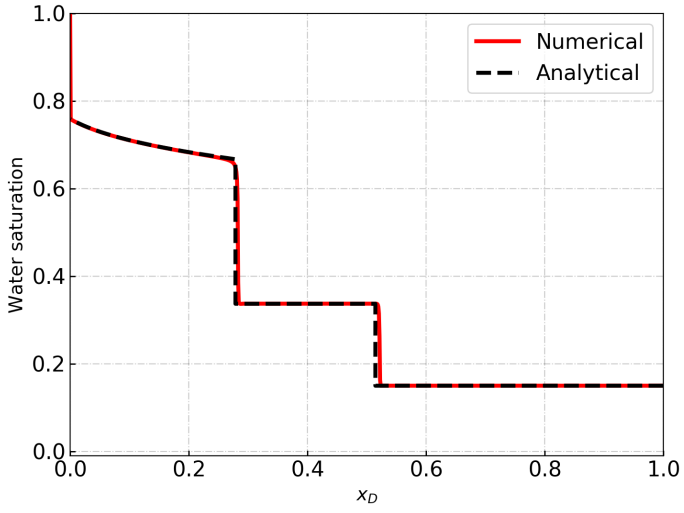

Figure 7 *Comparison between numerical solution and analytical solution with polymer injection at 0.20PV.*